THE JOURNAL OF PHYSICAL CHEMISTRY A

pubs.acs.org/JPCA

Feature Article

Role of Nonvalence States in the Ultrafast Dynamics of Isolated Anions

Jan R. R. Verlet,* Cate S. Anstöter, James N. Bull, and Joshua P. Rogers

Cite This: J. Phys. Chem. A 2020, 124, 3507−3519

Read Online

ACCESS | Metrics & More | Article Recommendations

ABSTRACT: Nonvalence states of neutral molecules (Rydberg states) play important roles in nonadiabatic dynamics of excited states. In anions, such nonadiabatic transitions between nonvalence and valence states have been much less explored even though they are believed to play important roles in electron capture and excited state dynamics of anions. The aim of this Feature Article is to provide an overview of recent experimental observations, based on time-resolved photoelectron imaging, of valence to nonvalence and nonvalence to valence transitions in anions and to demonstrate that such dynamics may be commonplace in the excited state dynamics of molecular anions and cluster anions.

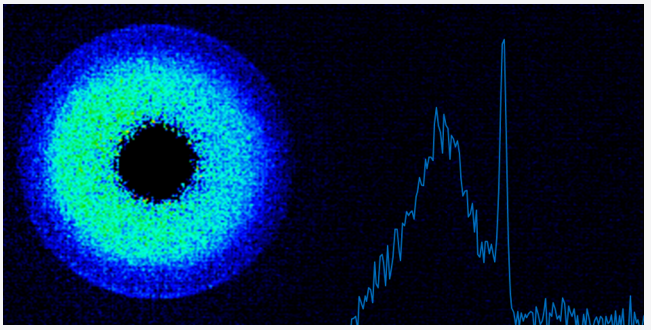

1. INTRODUCTION

Valence orbitals define molecular bonding and are therefore often considered the most important from a chemical perspective. But not all electrons occupy such orbitals. At the high-binding energy end of the scale, core electrons define the constituent atoms that make up molecules; at the very low binding-energy end, electronic states are associated with long-range potentials present in molecules. In neutral molecules, the Coulombic $-r^{-1}$ potential can bind an electron to its positive core. As the $-r^{-1}$ potential is a long-range potential, electrons that are weakly bound in such a potential are on average far away from the molecular cationic core. There is very little interaction with the cationic molecular core and, consequently, the nonvalence electronic states are essentially hydrogenic and form an infinite Rydberg series converging to the ionization limit. While Rydberg states have been a playground for physicists because of their remarkable properties including colossal polarizability and size,[1,2] they also play important roles in chemistry and in excited state dynamics.[3] Rydberg states often interact strongly with valence states to dictate the shape of their adiabatic potential energy surfaces and can partake in ultrafast internal conversion dynamics via conical intersections with valence states. The role of Rydberg states in ultrafast dynamics have been extensively discussed and studied. In stark contrast, the role of nonvalence states in the ultrafast internal conversion dynamics of anions has, until very recently, been effectively uncharted. The purpose of this Feature Article is to describe our recent efforts to bring to the fore the roles nonvalence states can play in the excited state dynamics of anions, be they photoexcited or electron-excited.

While a Rydberg electron is bound by the $-r^{-1}$ potential, this Coulombic potential is not present in an anion. Instead, weaker and shorter-range potentials are present, which can nevertheless bind an excess electron to the neutral core. For example, a neutral molecule possessing a large permanent dipole moment can bind an electron if, theoretically, the magnitude of the dipole moment $|\boldsymbol{\mu}| > 1.625$ D.[4−12] Experimentally, it has been found that the dipole moment should be $|\boldsymbol{\mu}| \gtrsim 2.5$ D. Much like a Rydberg state, the wave function of a dipole-bound state (DBS) has most of its amplitude away from the neutral molecular core. However, the DBS orbital is directional and is localized on the positive end of $\boldsymbol{\mu}$. Because of the much weaker and shorter-range potential compared to a Rydberg state, there is typically only a single-bound DBS with a binding energy on the order of a few to a few hundred millelectronvolts that generally scales with $|\boldsymbol{\mu}|$ of the neutral.

Beyond the e^-−$\boldsymbol{\mu}$ interaction, an excess electron can also be bound by higher order multipole moments. For example, quadrupole-bound states (QBS) have been predicted to exist in certain molecules and they have been recently observed experimentally.[13−15] A particularly interesting case is 1,4-dicyanocyclohexane anion for which a *cis*-conformer supports a

Received: February 13, 2020
Revised: March 26, 2020
Published: April 1, 2020

https://dx.doi.org/10.1021/acs.jpca.0c01260
J. Phys. Chem. A 2020, 124, 3507−3519

DBS and the *ee*-conformer supports a QBS.[15] An excess electron can also be bound in a nonvalence state by correlation forces. The most prominent example of such a nonvalence correlation-bound state (CBS) is predicted in C_{60}^-, with the nonvalence orbital extending well-beyond the valence orbital system of C_{60}.[16−19] Generally, however, it is a combination of all binding forces (dipole, mutipole, exchange, correlation) that leads to nonvalence state binding. For example, while a DBS may be dominated by the e^-−$\boldsymbol{\mu}$ interaction, correlation forces will also contribute and nonvalence states are generally assigned as DBS, QBS, or CBS depending on which of the forces dominate.

As the binding energy of nonvalence states in anions is typically very small, the nonvalence states lie energetically very close to the detachment threshold and the involvement of nonvalence states in excited state dynamics is therefore likely to arise when the valence excited states lie near this threshold. This is the case in a number of conjugated organic molecules. Because of the energetic proximity of the nonvalence state to the detachment threshold, nonvalence states are also important in electron capture of low energy electrons.[20−24] For example, it has been theorized that DBS act as a doorway to molecular anion formation in the interstellar medium.[25−27] Below, both cases of nonvalence participation in excited state dynamics and in electron capture are discussed.

2. PHOTOELECTRON IMAGING: AN IDEAL PROBE FOR NONVALENCE STATES

One of the most useful experimental methods for probing nuclear and electronic structure and dynamics of isolated molecules is photoelectron (PE) spectroscopy[28,29] and its time-resolved variant.[30,31] Photodetachment from anions is particularly convenient because the energy required to remove an electron from an anion is typically much lower than that for a neutral.[29] As photodetachment is essentially instantaneous, measurement of the electron kinetic energy, eKE, provides a direct measure of the energy difference between an initial anionic potential energy surface and a final neutral potential energy surface at the instantaneous geometry of the anion. The Franck−Condon factors determine relative intensities of vibrational levels and inform about the structural differences between the anion and neutral. In a time-resolved measurement, an initial short (femtosecond) pump pulse generates a nonequilibrium ensemble on an excited state potential energy surface whose evolution can be monitored using a second probe femtosecond pulse.[31,32] The time-resolved PE spectra contain both structural information (through changing Franck−Condon factors) and electronic state information through Koopmans correlations and energetic arguments.[33] In addition to the eKE spectrum, the use of PE imaging (i.e., velocity-map imaging[34]) yields PE angular distributions (PADs). These are sensitive to the orbital from which the electron was detached and, hence, together with the PE spectra, the PADs give information about the electronic character of the excited states being probed.[35−40] PADs are usually quantified using the anisotropy parameter, β_2, which has limiting values of +2, for a $\cos^2\theta$ distribution of the electron emission relative to the polarization axis of the light, and −1 for a $\sin^2\theta$ distribution.[41] Values between these two limiting cases introduce isotropy and when $\beta_2 = 0$, the distribution is purely isotropic. For a two-photon transition (as in pump−probe spectroscopy), an additional anisotropy parameter, β_4, is required because the first photon can induce alignment in the excitation. For all the data presented below, β_4 was measured but found to be essentially zero and so will not be discussed here.

While anion PE spectroscopy has been a powerful tool to probe anionic dynamics in a range of molecular systems, it has a particular sensitivity to nonvalence states. Because nonvalence states are weakly bound to the neutral core and have their electron density located predominantly outside of valence-electron density, the potential energy surface associated with the nonvalence state is very similar to that of the neutral core. This then dictates that the Franck−Condon factors are effectively diagonal and the resulting PE spectrum is spectrally very narrow.[42−47] Moreover, as the nonvalence orbital is much like a diffuse s-type atomic orbital, the PADs associated with photodetachment from a nonvalence state are distinctly aligned along the polarization axis of the probe pulse, $\beta_2 \rightarrow +2$. Finally, photodetachment from nonvalence states can have very large cross sections. The photodetachment cross-section becomes large when the size of the nonvalence orbital is similar to the de Broglie wavelength, λ_{dB}, of the outgoing electron.[42] For a 1.5 eV electron, λ_{dB} = 1.0 nm, which is comparable to the spatial extent of a typical nonvalence anionic orbital. Given that the nonvalence state is weakly bound, the production of an electron with eKE = 1.5 eV requires a photon of $h\nu \sim 1.5$ eV, which is perfectly suited to Ti:sapphire lasers that have a fundamental output at $h\nu$ = 1.55 eV (800 nm) and have been the workhorse of time-resolved spectroscopy.

The anions in our laboratory are produced either by electrospray ionization[39,48] or by electron impact ionization in a molecular beam.[49] An overview of our electrospray instrument is shown in Figure 1. Electrosprayed ions are thermalized to ∼300 K in a trap while anions produced in a molecular beam are colder but typically with a nonthermal distribution. Anions produced using either method are then injected into a time-of-flight mass-spectrometer. At the focus of the mass-spectrometer, a specific ion packet of known mass is subjected to light from an Nd:YAG pumped OPO or derived from a Ti:sapphire laser. The former allows easy tunability over the range $0.5 < h\nu < 6.2$ eV with laser pulses of ∼5 ns duration, while the latter offers short pulses with <50 fs duration. Electrons detached following the light-anion interaction are velocity-mapped in an imaging PE spectrometer.[34,50] PE imaging has important benefits over many other electron spectrometers, including: a near-unit collection efficiency of the electrons; the direct access to PADs as well as spectra; and a high sensitive to low energy electrons, which turns out to be very important in understanding the decay mechanism from nonvalence states. Full details of the experimental arrangements have been given elsewhere.[39,48]

By scanning $h\nu$ across the continuum and measuring PE spectra at each $h\nu$, a 2D map of the PE signal as a function of both $h\nu$ and eKE can be constructed. Such 2D PE spectra are particularly informative about the dynamics of anion resonances that are subject to autodetachment as well as competing nuclear dynamics. 2D PE spectroscopy represents the optical analogue of 2D electron energy loss spectroscopy (2D EELS)[51] with the important advantages that PE imaging also provides 2D PADs,[52−54,38,40,55] that time-resolved PE imaging can track the dynamics of electron-impact resonances,[53,54,56] and that it enables the study of mass-selected clusters.[57−61,49,62] The combination of 2D PE imaging and time-resolved PE imaging has been key to understanding the spectroscopy and dynamics of nonvalence states in anions and

https://dx.doi.org/10.1021/acs.jpca.0c01260
J. Phys. Chem. A 2020, 124, 3507−3519

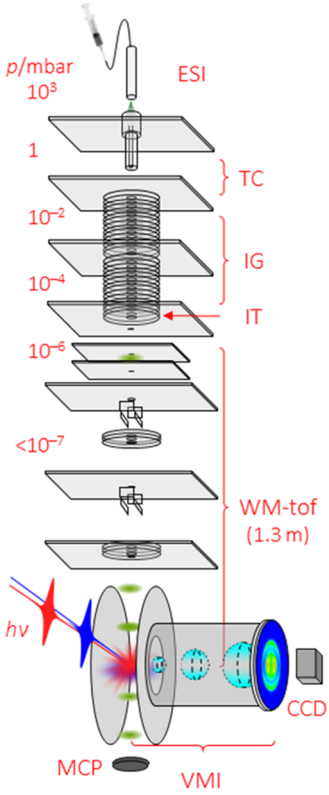

Figure 1. Schematic of anion photoelectron (PE) imaging spectrometer. Ions are generated by electospray ionization (ESI) and transferred into vacuum through a transfer capillary (TC). The ions enter a pair of ring-electrode ion guides (IG), which terminates in an ion trap (IT). Ions are ejected from the trap into a Wiley–MacLaren time-of-flight mass spectrometer (WM-tof). At the focus of the mass-spectrometer, mass-selected ions are intersected with light producing a PE cloud. The remaining anion beam is monitored on a multichannel plate (MCP) detector, while the electrons are directed using a velocity-map imaging (VMI) spectrometer onto a position sensitive detector. A charge-coupled device (CCD) captures the PE impacts and PE images are accumulated over many laser-shots. The pressures in various regions are indicated.

our early efforts in developing this methodology have been recently reviewed.[63]

3. VALENCE TO NONVALENCE DYNAMICS

3.1. Open-Shell Cluster Anions. The involvement of nonvalence states in the nonadiabatic dynamics of valence excited states was first observed in the radical anion cluster of coenzyme Q_0, $(CQ_0)_2^-$.[57] CQ_0 is biologically relevant derivative of *para*-benzoquinone, which have been of interest because of their electron accepting abilities that are mediated by ultrafast internal conversion dynamics between valence-localized resonances.[52,64] Excitation of $(CQ_0)_2^-$ to a π^* resonance just above the detachment threshold showed unexpected structure in the PE signal peaking near eKE = 0 eV, across a range of photon energies (Figure 2a). Very low energy PE signal is commonly taken as evidence of thermionic emission in which the ground electronic state of the anion is recovered and electrons are statistically emitted on a long (microsecond to millisecond) time scale.[65,66] However, as thermionic emission is statistical in nature, its kinetic energy distribution should be Boltzmann-like,[67] which is in stark contradiction to the PE spectra shown in Figure 2a. The origin of the structure in the low energy PE signal was uncovered by measuring the time-resolved PE spectra following excitation to π^* resonances that are located near the detachment threshold. These data are shown in Figure 2b, following excitation at 3.10 eV and a probe at 1.05 eV. Note that we also performed the experiment with a 1.55 eV probe, but the probe accessed a resonance leading to additional dynamics. At early times, the pump–probe PE signal is broad and consistent with photodetachment from a valence resonance in which the excited state surface is different to the neutral surface leading to a broad Franck–Condon window. The data taken at $h\nu_{probe}$ = 1.55 eV offered better time resolution and showed the broad feature more pronouncedly than in Figure 2b, but it also led to additional dynamics that complicated the analysis of the low eKE peak. As time progresses, the broad PE feature sharpens, leaving a spectrally narrow peak at eKE ~ $h\nu_{probe}$. Moreover, the PAD associated with this narrow peak had an anisotropic distribution peaking along the polarization axis as shown in Figure 2c. As discussed above, a narrow spectral distribution, small binding energy, and predominantly p-wave angular momentum following photodetachment, all point to the formation of a nonvalence state. This nonvalence state PE signal then decayed with a lifetime of ~2 ps.

In addition to the appearance and decay of PE signal in the pump–probe experiments, the probe also leads to a decrease in the structured signal observed at low eKE (Figure 2b). As a function of pump–probe delay, this bleached signal recovers with the same lifetime as the nonvalence state decays. Hence, this shows that the signal at low-eKE arises from the nonvalence state. The electron ejection mechanism involves autodetachment as the total energy of the system remains above the adiabatic energy. Because the autodetachment lifetime of the nonvalence state is ~2 ps, the mechanism is nonstatistical. But where does the structure in the autodetachment spectrum come from?

First, we consider the nature of the nonvalence state. Ground state calculations on both the anion and neutral showed that the lowest energy structures of the clusters had $|\boldsymbol{\mu}|$ > 5 D. Hence, the most likely nonvalence state would be a DBS and indeed calculations did find a DBS in the cluster. Returning to the origin of the structure at low eKE, for this to be observed would suggest that the autodetachment was promoted by specific vibrational modes. Theory and experiment have shown that the propensity rule in autodetachment from a nonvalence state to form the neutral is to lose one quantum of vibrational energy, $\Delta v = -1$.[68,69] The root of the rule comes from the near-diagonal Franck–Condon factors between the two surfaces, as shown in Figure 3. Hence, if specific vibrational modes lead to autodetachment, then the PE spectrum can show vibrational structure associated with these vibrations. The vibrations that promote autodetachment have been considered in detail by Simons[68] and, in a zeroth-order picture, can be thought of as those vibrations that are strongly coupled to the DBS orbital. As the DBS is bound by $\boldsymbol{\mu}$, it is the vibrations that strongly modulate $\boldsymbol{\mu}$ (i.e., IR active modes) that are the prime candidates. For $(CQ_0)_2^-$, because the cluster is large and with many low-frequency modes, there were many possible modes that satisfied this criterion such that the identification of specific modes was impossible. An overall picture of the dynamics is provided in Figure 4, showing the origin of the initial broad distribution for a valence-localized resonance that then leads to the narrow distribution of the nonvalence state and its subsequent autodetachment.

https://dx.doi.org/10.1021/acs.jpca.0c01260
J. Phys. Chem. A 2020, 124, 3507–3519

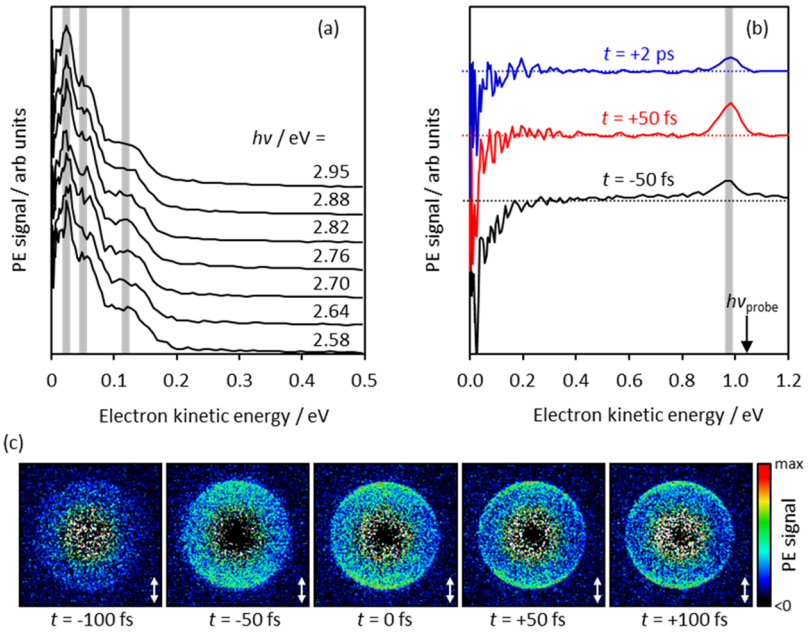

Figure 2. Valence to nonvalence dynamics in $(CQ_0)_2^-$. (a) Photoelectron (PE) spectra taken at a number of photon energies showing a common structured PE spectrum. (b) Representative time-resolved PE spectra following excitation to π^* resonances at three different delays, showing a broad PE spectrum at the earliest times, which rapidly evolves into a narrow PE spectrum at eKE ~ $h\nu_{probe}$ = 1.05 eV (assigned to photodetachment from a nonvalence state). This signal then decays at longer times. Concomitant to these dynamics is depletion of the signal shown in (a) which recovers over time. (c) Representative time-resolved raw PE images (from which data in (b) is derived), showing the evolution of the PE images and anisotropy associated with the nonvalence state. Vertical double arrows indicate the polarization axis.

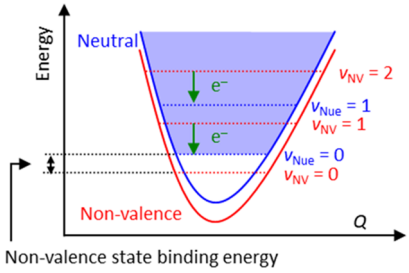

Figure 3. Schematic showing origin of $\Delta v = -1$ autodetachment propensity rule. The potential energy surfaces of the neutral and nonvalence state are parallel and offset by the binding energy of the nonvalence state. Vibrational levels of the nonvalence state decay by detaching an electron leaving the neutral with one less quantum of vibrational energy.

Very similar valence to nonvalence dynamics to those seen in $(CQ_0)_2^-$ were seen in the radical anion trimer of *para*-toluquinone, $(pTQ)_3^-$.[59] An overview of the results are shown in Figure 5. Excitation to the analogous π^* resonances led to a similar, structured low eKE spectrum in the one-color PE spectra just above the adiabatic detachment energy. In the time domain, initial dynamics were characterized by a broad transient PE spectrum that is representative of a valence-localized excited state (associated with the π^* resonance) that then evolves rapidly into a narrow spectral feature with eKE ~ $h\nu_{probe}$ and with a PAD characteristic of a nonvalence state. Concomitant to this, the structured low-eKE feature was bleached by the probe, showing that the nonvalence state decays by vibrational autodetachment. The dynamics followed a similar picture, as shown in Figure 4. However, a key

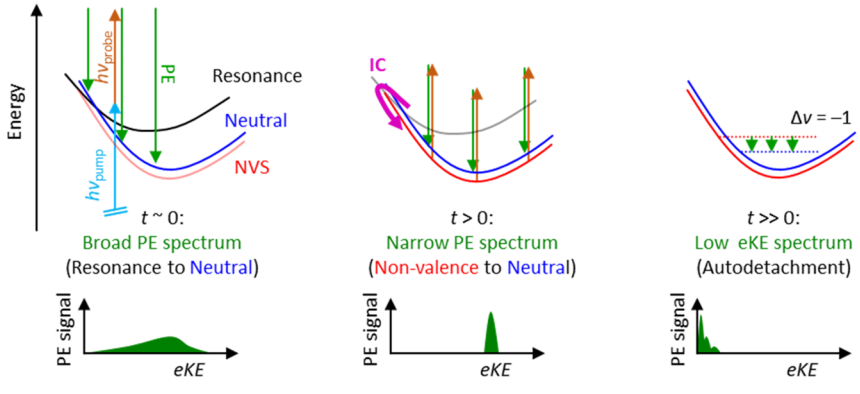

Figure 4. Schematic describing valence to nonvalence dynamics. At $t \sim 0$, a valence resonance is excited by $h\nu_{pump}$ and probed with $h\nu_{probe}$. The resulting photoelectron (PE) spectrum is broad because of the differing geometries of the resonance and neutral. At $t > 0$, the resonance converts to the nonvalence state, leading to a narrow PE spectrum as the energy gap between nonvalence state and neutral is (relatively) invariant on geometry. At $t \gg 0$, mode-specific vibrational autodetachment commences and leads to a structured PE spectrum at low eKE.

https://dx.doi.org/10.1021/acs.jpca.0c01260
J. Phys. Chem. A 2020, 124, 3507−3519

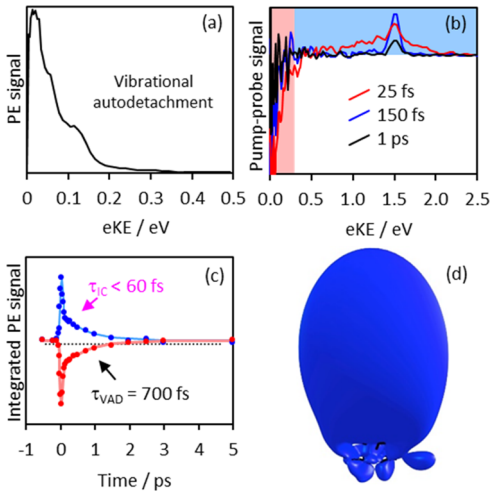

Figure 5. Valence to nonvalence dynamics in $(pTQ)_3^-$. (a) Photoelectron (PE) spectrum taken averaged over a number of photon energies near threshold, showing a common structured PE spectrum. (b) Representative time-resolved PE spectra following excitation to π^* resonances at three different delays, showing a broad PE spectrum at the earliest times, which rapidly evolves into a narrow PE spectrum (assigned to photodetachment from a nonvalence state) and then decays at longer times. Concomitant to these dynamics is depletion of the signal shown in (a) which recovers over time. (c) Integrated PE signal over regions indicated in (b), with the blue representing the pump−probe signal and the red the bleached low energy signal shown in (a). (d) Nonvalence orbital, which is dominated by correlation forces.

difference between $(CQ_0)_2^-$ and $(pTQ)_3^-$ is that the latter does not appear to have a sufficiently large permanent dipole moment to support a DBS. Extensive structural searches indicated that the dipole moment in either the neutral or anion geometries was $|\mu| < 1.2$ D. Nevertheless, our calculations did show that a nonvalence state exists in the cluster anions, with correlation as the dominant nonvalence binding force. Hence, while the dipole moment (and quadrupole moment) contributes to the overall binding of the nonvalence state, it is predominantly a nonvalence CBS and the study served as the first direct experimental observation of such a state. Figure 5d shows the nonvalence CBS orbital calculated for this cluster.

3.2. Bioactive Chromophore Anions. While the above dynamics have been observed in molecular clusters, it would seem logical that similar processes could also occur in purely covalent molecular anions. In particular, whenever valence excited states are located near the detachment threshold, such valence to nonvalence internal conversion dynamics could be operable as long as the corresponding neutral has a sufficiently large dipole (or multipole) moment. It turns out that a number of interesting molecular anions have such an electronic structure, including anionic chromophores of photoactive proteins, several of which have their $S_1(\pi\pi^*)$ state close to the adiabatic detachment energy. Examples include the *para*-HBDI chromophore in green fluorescent protein (GFP)[70,71] and the *para*-cinnamate chromophore in photoactive yellow protein (PYP). However, time-resolved PE spectroscopy of the model chromophore in GFP[72] and a model chromophore of PYP[73] showed no evidence for internal conversion to a nonvalence state. Very recently though, we showed evidence for participation of a nonvalence state in a slightly different derivative of the PYP chromophore.[74]

A selection of the time-resolved PE spectra for the deprotonated methyl ester of *para*-coumaric acid (pCEs$^-$, Figure 6) following excitation at $h\nu$ = 2.83 eV and probing at

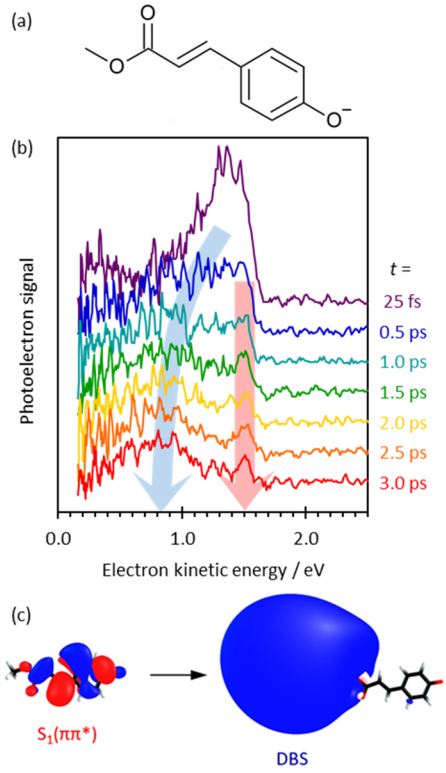

Figure 6. Valence to nonvalence dynamics in pCEs$^-$. (a) Molecular structure of pCEs$^-$. (b) Representative time-resolved photoelectron (PE) spectra flowing excitation to the bright $S_1(\pi\pi^*)$ state. Isomerization dynamics on the $S_1(\pi\pi^*)$ state surface leads to a red shift of the PE signal (blue arrow). Concomitant to this, a narrow PE signal appears at eKE ~ $h\nu_{probe}$ = 1.55 eV, which subsequently decays. This narrow signal arises from photodetachment from the nonvalence state of pCEs$^-$. (c) Molecular orbitals associated with the valence $S_1(\pi\pi^*)$ and the nonvalence dipole-bound states.

$h\nu$ = 1.55 eV is shown in Figure 6.[74] The excitation energy was chosen to coincide with the adiabatic detachment energy (measured to also be 2.83 eV). At early times, the PE spectrum is relatively broad, indicative of a valence-localized state (i.e., the $S_1(\pi\pi^*)$ state). This shifts toward lower eKE and broadens with time and reflects the geometric change taking place on the excited state surface. Specifically, excitation leads to a weakening of the conjugated *trans* configuration of pCEs$^-$, which results in rotation of the central bonds. Indeed, the dynamics of the PE spectra are similar to those observed for the GFP chromophore anion.[72] However, the time-resolved PE spectra also reveal a narrow feature at eKE ~ $h\nu_{probe}$, which becomes more apparent at t > 1 ps in Figure 6. The PADs again point to this peak being a nonvalence state. But, unlike in the cluster cases, where essentially all population was transferred from valence to nonvalence states, in pCEs$^-$, it appears that only a fraction is transferred to a nonvalence state. Hence, the wavepacket on the $S_1(\pi\pi^*)$ state bifurcates with some population remaining on the valence state and undergoing excited state isomerization, while the rest of the population becomes trapped in the nonvalence state. The subsequent decay of the nonvalence state is similar to that in clusters and proceeds by vibrational autodetachment on a time

https://dx.doi.org/10.1021/acs.jpca.0c01260
J. Phys. Chem. A 2020, 124, 3507−3519

scale of ∼3 ps. The valence state population remains on the excited state surface for longer and also decays by autodetachment with a lifetime of ∼45 ps. Again, the pictorial representation of the dynamics in Figure 4 is mostly valid, with some modifications required to incorporate the bifurcation of the excited state wavepacket.

The observation of internal conversion from a valence to a nonvalence state in *p*CEs$^-$ presents the first observation of such a transition in a closed-shell molecular anion. It is enabled by the energetic proximity of the $S_1(\pi\pi^*)$ state to the detachment threshold and therefore also nonvalence states. While this proximity may appear to be a fortuitous coincidence, it is in fact a relatively common feature of many conjugated organic anions of biological relevance. The detachment threshold of many phenolate derivatives lies around 2−3 eV,[38] which is also in the range of the $S_1(\pi\pi^*)$ state. Moreover, the $S_1(\pi\pi^*) \leftarrow S_0$ transition has a quite broad spectral range because of the difference in geometry between S_0 and S_1. Hence, the coincidence is perhaps not that fortuitous. Indeed, we have now seen internal conversion between valence and nonvalence states in other conjugated organic anions, which will be reported on in the near future.

3.3. Valence to Nonvalence Transition Mechanism. In the above, we have demonstrated that valence π^* resonances can form nonvalence states. However, we have not commented in detail on the mechanism. When a nonadiabatic transition between two electronic states is observed that occurs on a subpicosecond time scale, a conical intersection is generally invoked to explain such a transition.[75] We have done the same in the above work and this is likely to be a valid picture for the dynamics described above. For example, in *p*CEs$^-$, our calculations could identify possible geometric changes that could facilitate a conical intersection.[74] One involved a crossing of the $S_1(\pi\pi^*)$ surface with the DBS surface along the Franck−Condon active vibrational mode, while another along an internal rotation coordinate associated with the isomerization occurring on the $S_1(\pi\pi^*)$ surface. Unfortunately, the experiments could not verify which, if any, is correct. However, in the spirit of a Feature Article, we also put forward here an alternative mechanism that could facilitate the nonadiabatic transition from valence to nonvalence states.

In all cases presented above, the valence state is a π^* resonance and therefore autodetachment from this resonance is an open channel. Moreover, as the valence resonance is energetically close to the adiabatic detachment energy of the anion, the kinetic energy of the outgoing electron is likely to be small. Hence, as autodetachment proceeds, the partial wave (predominantly of s-character at low eKE because of the centrifugal barrier[76]) leaves the neutral core. As it does so, $\boldsymbol{\mu}$ and/or correlation forces may be sufficiently large to "recapture" the electron on its way out into a nonvalence state. In essence, this is similar to the reverse process of electron capture through nonvalence states that is discussed below. Such a mechanism is different to internal conversion through a conical intersection because it also involves the detachment continuum.

4. NONVALENCE TO VALENCE DYNAMICS

4.1. Nonvalence States in Electron Attachment to a Molecule. In the above, direct time-resolved spectroscopic evidence for valence to nonvalence transitions were presented. But if the nonadiabatic coupling between a valence and nonvalence state is large to enable such a transition, then the reverse transition of nonvalence to valence should also be possible. This is believed to be an important mechanism in electron capture where a nonvalence state can serve as a "doorway" state for a slow incoming electron leading to a valence-bound anion.[20,22,25] As the doorway nonvalence state is a transient species, time-resolved PE spectroscopy is ideally suited to capture spectroscopic signatures of such dynamics. As a source of slow electrons, Johnson and workers have shown that iodide, I^-, can be very useful.[77−83] Specifically, iodide clusters with neutral molecules, $I^-\cdot M$, exhibit charge-transfer bands in which the charge is injected from the iodide into the neutral M. Perhaps the best known example is when M is a water cluster in which case the charge-transfer band is called a charge-transfer-to-solvent (CTTS) band.[82] The CTTS state has an orbital that is supported by the instantaneous combined dipole moment of the water molecules and therefore can be thought of as a DBS.[84] In water, this then leads to the formation of a hydrated electron,[85−87] but the same principles extend to situations where M is a simple molecule. A particularly elegant example of dynamics was reported by the Neumark group for M = nitromethane,[88] and they have since applied this method to probe electron attachment dynamics to nucleobases.[89−92] In certain nucleobases, a DBS serves as the doorway state that then evolves into valence states of the nucleobase; this work has been reviewed recently and the reader is referred to this this for more details.[92] Here, we focus on work in our group probing the electron capture dynamics through the nonvalence CBS in hexafluorobenzene, C_6F_6, to form the valence-bound anion, $C_6F_6^-$.[24]

The work was motivated by a computational study by Voora and Jordan who showed that a nonvalence CBS state of $C_6F_6^-$ can adiabatically lead to the formation of the valence-bound $C_6F_6^-$.[23] Neutral C_6F_6 is planar and, thus, the nonvalence CBS has a planar neutral core associated with it. In contrast, valence-bound $C_6F_6^-$ has the excess electron in a valence orbital, which causes a Jahn−Teller distortion that leads to a buckled nuclear geometry.[23,49,93] Hence, the geometric coordinate adiabatically connecting the nonvalence CBS to the valence-bound anion is this out-of-plane buckling coordinate. Experimentally, the nonvalence CBS can be accessed by charge transfer from iodide in the $I^-\cdot C_6F_6$ cluster because C_6F_6 in the cluster has a planar geometry and is essentially neutral with most of the charge residing on the iodide. We generated the cluster anion in a molecular beam source and used femtosecond pulses at 3.10 eV to excite to the charge-transfer state. Our calculations show that this charge-transfer state has the appearance of the nonvalence CBS, suggesting that, indeed, the nonvalence state is initially populated. The dynamics were subsequently probed using 1.55 eV, and the results are reproduced in Figure 7.[24]

The time-resolved PE spectrum is shown in Figure 7a. At early times, a narrow PE feature is observed centered at eKE = 1.10 eV. This feature decays very rapidly (within the time-resolution of the experiment, ∼40 fs) and appears to shift to lower eKE and broaden substantially. At about 180 fs, the PE signal in the range 0.25 < eKE < 0.60 eV is no longer visible, but it then returns at ∼300 fs before disappearing again and reappearing. The dynamics associated with this signal (PE signal integrated over 0.25 < eKE < 0.60 eV range) is shown in Figure 7c and clearly shows this oscillation. The oscillation can be fit to a decaying cosine function with a frequency of 121 cm^{-1} (period is 275 fs) but required a phase shift of −0.6 radians (equivalent to ∼30 fs). The measured frequency of the

https://dx.doi.org/10.1021/acs.jpca.0c01260
J. Phys. Chem. A 2020, 124, 3507−3519

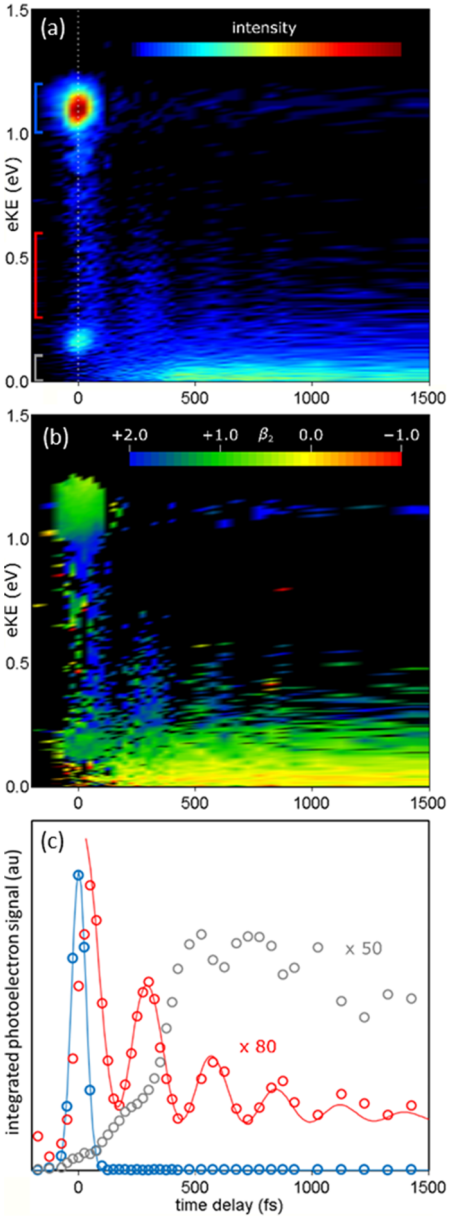

Figure 7. Dynamics in $I^-C_6F_6$ following charge-transfer excitation. (a) Time-resolved photoelectron (PE) spectra probed at $h\nu_{probe}$ = 1.55 eV as a false-color intensity plot with t = 0 indicated by a vertical dashed line. (b) Time-resolved anisotropy parameters, β_2 (blacked-out regions have a PE signal <4% of signal in (a)). (c) Integrated PE signal (open circles) over spectral windows indicated by the correspondingly colored square brackets in (a). Fits are shown in solid lines.

oscillation matches the vibrational mode that leads to a buckling of C_6F_6 and the time-resolved PE spectrum can be explained using the potential energy surfaces shown in Figure 8. At early times, the nonvalence CBS is formed leading to a narrow PE spectrum. As time evolves, the system begins to buckle. As it does, the energy of the valence state of $C_6F_6^-$ decreases while that of the neutral C_6F_6 final state increases. Hence, a decrease in eKE is observed in the dynamic PE spectra. At the outer turning point of the buckling coordinate, the probe ($h\nu$ = 1.55 eV) does not have enough energy to access the neutral and the PE signal disappears. It then returns to the inner turning point (i.e., mostly planar) and the PE

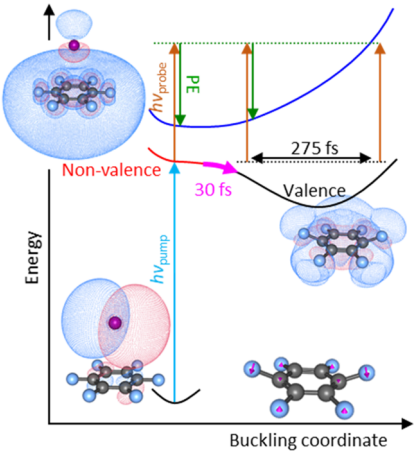

Figure 8. Schematic of dynamics in $I^-C_6F_6$. Excitation of $I^-(5p)$ with $h\nu_{pump}$ accesses a charge-transfer state that represents the nonvalence state of $C_6F_6^-$. The $h\nu_{probe}$ leads to a narrow photoelectron (PE) spectrum. This nonvalence correlation-bound state then evolves on a 30 fs time scale into the valence state of $C_6F_6^-$, through an out-of-plane bucking coordinate associated with a Jahn−Teller distortion. The butterfly mode has a period of 275 fs. With $h\nu_{probe}$, the PE spectrum at the inner turning point (planar) leads to a broad PE spectrum. With high eKE and at the outer turning point, no PE is seen.

signal returns as the eKE increases, before disappearing again at the outer turning point. The amplitude of the oscillation decreases predominantly because internal vibrational redistribution (IVR) of energy takes place and the dominant buckling vibration leaks into the many other modes of the anion. IVR also leads to the appearance of the signal at low eKE (<0.2 eV), which comes about from the excitation of excited valence states of $C_6F_6^-$ by the probe.[49]

The only aspect that remains to be explained is the phase-shift required to fit the oscillatory dynamics of the valence state of the anion (Figure 7c). The 30 fs corresponds to a delay in the formation of the valence state and thus likely corresponds to the transition from nonvalence to valence states of $C_6F_6^-$. Indeed, close inspection of the PADs in Figure 7b provides some evidence for this. At early times, the PE spectrum associated with the nonvalence CBS has a PAD that is characterized by $\beta_2 \sim 1$. Signal at lower eKE has a PAD characterized by $\beta_2 \sim 2$. The latter corresponds to the β_2 measured (and expected) for detachment from the valence state of $C_6F_6^-$.[49] For a nonvalence state, β_2 is typically around 1 and so the change in β_2 is a direct measure of the change in molecular orbital from the nonvalence CBS to the valence state of $C_6F_6^-$. In fact, the 30 fs shift is also apparent in the time-resolved PE spectra as a slight shift with respect to t = 0 as shown in Figure 7a.

4.2. Nonvalence States in Electron Attachment to Clusters. As already commented on above, clusters are an important case of electron capture, in part because they provide a link to the bulk. The most-studied example is that of electrons injected into water, which has been studied by Neumark and co-workers using time-resolved PE spectroscopy of $I^-\cdot(H_2O)_n$.[85,87,94,95] However, evidence for electron capture can also be found in the PE spectra of homomolecular clusters.[49,62,96] Figure 9 shows the 2D PE spectra of $(C_6F_6)_n^-$.[62] Two direct detachment channels are apparent in the PE spectroscopy of $C_6F_6^-$. The first leads to the formation of the neutral ground state. This is a broad feature because the

https://dx.doi.org/10.1021/acs.jpca.0c01260
J. Phys. Chem. A 2020, 124, 3507−3519

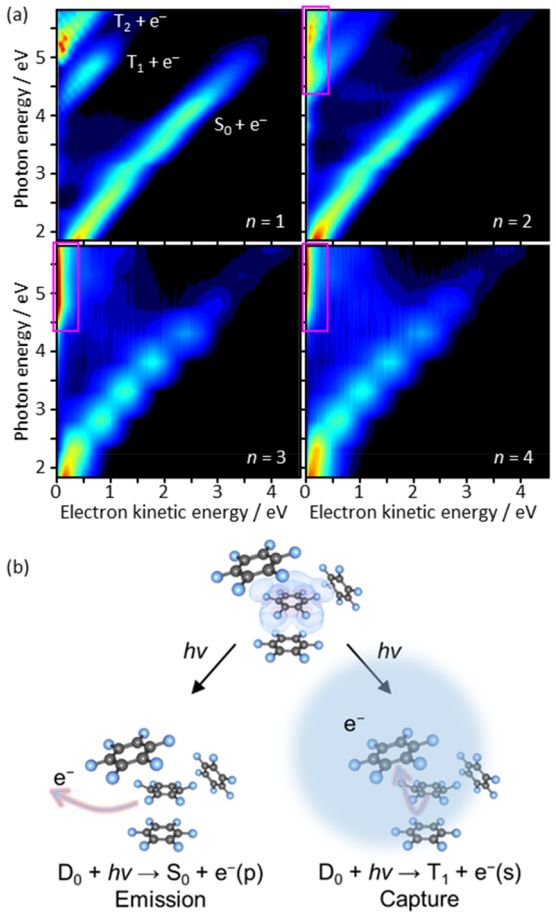

Figure 9. Nonvalence state dynamics in $C_6F_6^-$ clusters. (a) 2D photoelectron (PE) spectra of $(C_6F_6)_n^-$ with n = 1−4. The pink square for $n \geq 2$ indicates an observed low energy emission channel that opens when the triplet of the neutral is accessed. (b) Schematic diagram of proposed PE emission when forming the S_0 neutral and recapture by a nonvalence state when forming the T_1 (and T_2) in the neutral.

valence state of $C_6F_6^-$ has a geometry very different from that of C_6F_6 (i.e., the Jahn−Teller distortion). A second direct detachment channel can be seen around $h\nu \sim 4$ eV. This corresponds to the formation of the neutral in its first triplet excited state, T_1, with a third channel corresponding to the T_2 state. In the clusters, these direct detachment channels are also visible, however, for $n \geq 2$, an additional feature at low eKE is seen when the T_1 channel becomes available. As highlighted in the above discussions, low eKE PE signal is seen when a resonance is excited that leads to vibrational autodetachment or thermionic emission. However, in $(C_6F_6)_n^-$, there is no evidence that a resonance is excited, and even if there was, why would the appearance of low eKE signal be correlated with the opening of the T_1 channel? The latter point is particularly puzzling at first glance because in forming the final state of the neutral, the electron has already departed and so how can it lead to low eKE PE signal?

The only reasonable explanation we could arrive at was that this low eKE signal arises from recapture of the outgoing PE by a nonvalence state of the cluster. Specifically, the charge is quite localized on a C_6F_6 monomer in the $(C_6F_6)_n^-$ cluster so that a departing electron will "see" a number of neutral (planar) C_6F_6 molecules, which we have shown in the previous section can accept low energy electrons through their nonvalence CBS. But why is the nonvalence CBS not involved for the S_0 channel but it is for the T_1/T_2 channel? The PADs provide a hint into this. The emission when accessing the S_0 neutral state is characterized by $\beta_2 \sim 2$: the outgoing wave is essentially a pure p-wave. The PADs associated with detachment channel forming either T_1 or T_2 are much closer to isotropic suggesting that the outgoing PE has a significant s-wave contribution. In an electron capture process, the symmetry of the electron is important and as the nonvalence correlation-bound state is predominantly of s-character, it follows that s-wave attachment may be more favorable than p-wave attachment. As the formation of the S_0 ground state in photodetachment produces electrons of p-wave character, the nonvalence CBS cannot capture the outgoing electron, while for the T_1 channel, it can. The recapture can lead to either vibrational autodetachment from the nonvalence CBS leading to slow electrons or can lead to the formation of valence-bound anions with the subsequent ejection of electron by thermionic emission. Unfortunately, we did not have the required signal-to-noise to perform time-resolved PE imaging experiments, which would be able to clearly identify the invoked electron recapture process and ultimate autodetachment mechanism.

4.3. Comment on the Nonvalence to Valence Transition Mechanism in I^-·M. Figure 8 implies an adiabatic transition from nonvalence to valence state following photoexcitation of $I^-\cdot C_6F_6$. The same overall picture has also been used in the work by Neumark and co-workers to describe the photoexcitation of I^-·M, where M is a nucleobase.[92] However, we note that the final state of the reaction, $I{\cdot}M^-$, is simply a local minimum on the same adiabatic potential energy surface as I^-·M. That is to say, both are in the ground electronic state. Photoexcitation cannot access the ground state and a nonadiabatic transition must take place between the initially excited "charge-transfer" state and the final valence-bound state of M^-. Indeed, this is well-known for the case where M = $(H_2O)_l$. Chergui and co-workers showed that the CTTS of $I^-_{(aq)}$ fluoresces,[97] in agreement with the interpretation of the phase-resolved transient second-harmonic generation of $I^-_{(aq)}$ at the water/air interface.[98,99] The same fluorescence will be present when M = $(H_2O)_n$ or a molecule. Hence, the overall picture shown in Figure 8 is in fact somewhat more complex.

Finally we briefly comment that nonvalence to valence transitions may also be possible in isolated molecular anions. In the above, only clusters were considered, be they I^-·M or simply molecular cluster anions. A recent PE spectroscopy study by the Wang group has provided some evidence for a nonadiabatic transition from a nonvalence DBS to a triplet state in the deprotonated 4,4′-biphenol anion.[100] This not only implies that nonvalence to valence transitions may be important in intramolecular excited state dynamics of anions, but also that intersystem crossing pathways may be readily accessed.

5. SUMMARY AND OUTLOOK

The main purpose of this Feature Article is to highlight that nonvalence states actively participate in the nonadiabatic dynamics of excited states of anions and that time-resolved PE imaging serves as an ideal spectral tool to probe their dynamics. Valence to nonvalence state internal conversion is important in photoexcited processes while nonvalence to valence transitions are important in electron capture processes. The participation of nonvalence states has so far only been

https://dx.doi.org/10.1021/acs.jpca.0c01260
J. Phys. Chem. A 2020, 124, 3507−3519

seen in a relatively small number of systems. However, we note that a relatively small number of anions have been studied by time-resolved PE spectroscopy and the signatures of nonvalence states in single-photon PE spectra are not obvious. Hints for nonstatistical autodetachment processes can sometimes be seen in the low eKE PE spectra, but such fingerprints do not guarantee that nonvalence states are responsible. It is only through the use of time-resolved PE spectroscopy and particularly imaging that a "smoking gun" can be found.

The observations and understanding of the role of nonvalence state in anions is still in its infancy. From an experimental perspective, studies to date have focused on rather complex anions making assignment of specific vibrational modes in the autodetachment or uncovering detailed internal conversion mechanism difficult. From a theoretical perspective, the problem is a challenging one: calculating nonadiabatic dynamics for excited states and very weakly bound states of anions that are buried in an autodetachment continuum is far from trivial. Nevertheless, much effort has been directed recently to developing electronic structure methods to deal with such problems.[101]

While we hope that we have shown that nonvalence states in anions are not a mere academic curiosity, a critical question related to the role of nonvalence states is whether they are relevant in condensed phases. To some extent, cluster work can begin to address these questions and certainly, for $I^-(H_2O)_n$ one can draw clear parallels with analogous dynamics in the bulk[102] or on surfaces.[98,99] The main effect of an environment is to increase the electron detachment energies. As the nonvalence state is weakly bound, this also means that the nonvalence states shift dramatically with respect to the ground (valence) state. Hence, the nonvalence states in, for example, isolated chromophores of photoactive proteins are not likely to be important for the S_1 state, but they may be for higher-lying excited states where they could be important precursors to photo-oxidation.[56,103] As an example, the absorption spectrum of the GFP chromophore suggests that the binding pocket in the protein is more accurately resembled by a vacuum than a solvent[71,104] such that there may be sufficient space to accommodate a nonvalence state.[105] We have recently shown that the excluded volume imposed by an aliphatic (noninteracting) chain does not appear to destroy a nonvalence state,[106] although it is clear from theoretical considerations that the excluded volume does influence the binding energy of a nonvalence state.[107] Nevertheless, if the space is restricted in a soft-matter environment, nonvalence states associated with an anion may still be present. We note that photo-oxidation of GFP has been observed following UV excitation,[108] which requires tunnelling through the protein.[109,110] This would certainly be enhanced through a molecular orbital that acted as a doorway for electron transfer.

AUTHOR INFORMATION

Corresponding Author

Jan R. R. Verlet − *Department of Chemistry, Durham University, Durham DH1 3LE, United Kingdom;* orcid.org/0000-0002-9480-432X; Email: j.r.r.verlet@durham.ac.uk

Authors

Cate S. Anstöter − *Department of Chemistry, Durham University, Durham DH1 3LE, United Kingdom*

James N. Bull − *School of Chemistry, University of East Anglia, Norwich NR4 7TJ, United Kingdom;* orcid.org/0000-0003-0953-1716

Joshua P. Rogers − *Department of Chemistry, Durham University, Durham DH1 3LE, United Kingdom*

Complete contact information is available at: https://pubs.acs.org/10.1021/acs.jpca.0c01260

Notes

The authors declare no competing financial interest.

Biographies

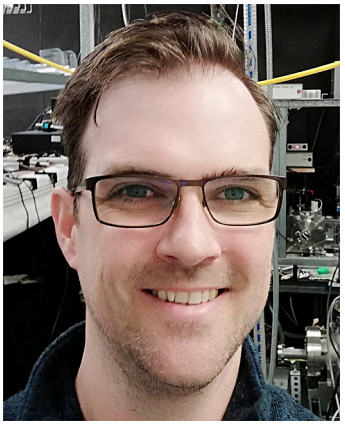

Jan R. R. Verlet received an MSci in Chemistry in 1999 and a Ph.D. from King's College London in 2003 under the supervision of Prof. Helen H. Fielding. Following a postdoctoral position with Prof. Daniel Neumark at UC Berkeley, he started his independent career at Durham University in 2006 as a lecturer and an EPSRC Advanced Research Fellow and became a full professor in 2016. His research interests are in the spectroscopy and excited state dynamics of anions in the gas phase, at interfaces and in condensed phases.

Cate S. Anstöter received her MChem from the University of Sheffield in 2014, her MPhil in Physical Chemistry from the University of Manchester in 2015, and her Ph.D. from Durham University in 2019. Her Ph.D. thesis was on "Probing the Electronic Structure and Dynamics of Anions in the Gas Phase" working under the supervision of Prof. Jan Verlet. During her Ph.D., she was awarded a grant by the Russian Foundation for Basic Science to work with Prof. Anastasia Bochenkova at Moscow State University for three months. Cate is currently a postdoctoral fellow at Temple University under the supervision of Prof. Spiridoula Matsika.

https://dx.doi.org/10.1021/acs.jpca.0c01260
J. Phys. Chem. A 2020, 124, 3507−3519

James N. Bull studied Chemistry at the University of Canterbury, New Zealand, graduating with a BSc. (Hons) in 2007 and a Ph.D. in 2010. He then moved to Oxford University on a Marie-Curie Fellowship to work in the group of Prof. Claire Vallance, studying the dynamics of electron impact ionization. In 2013, James joined the group of Prof. Jan Verlet at Durham University, applying photoelectron spectroscopy to study isolated anions. James then relocated to Australia, where he worked in the group of Prof. Evan Bieske at the University of Melbourne, applying tandem ion mobility mass spectrometry coupled with laser spectroscopy to investigate the photochemistry of shape-selected ions. James started as a lecturer at University of East Anglia in 2019 where he is developing and applying action spectroscopy techniques to study isolated ions.

Joshua P. Rogers received his MSc in Physics and Chemistry at Durham University in 2013 and continued there to complete his Ph.D. in Chemistry under the supervision of Prof. Jan Verlet in 2017. Now in the Department of Physics, Josh is a postdoctoral fellow in solid-state quantum optics under the supervision of Prof. Matthew Jones.

■ ACKNOWLEDGMENTS

We are grateful for funding from the European Research Council (Starting Grant 306536) and Durham University.

■ REFERENCES

(1) Stebbings, R. F.; Dunning, F. B. *Rydberg States of Atoms and Molecules*; Cambridge University Press, 1983.
(2) Gallagher, T. F. *Rydberg Atoms*; Cambridge University Press, 1994.
(3) Reisler, H.; Krylov, A. I. Interacting Rydberg and Valence States in Radicals and Molecules: Experimental and Theoretical Studies. *Int. Rev. Phys. Chem.* **2009**, *28* (2), 267−308.
(4) Fermi, E.; Teller, E. The Capture of Negative Mesotrons in Matter. *Phys. Rev.* **1947**, *72* (5), 399−408.
(5) Zimmerman, A. H.; Brauman, J. I. Resonances in Electron Photodetachment Cross Sections. *J. Chem. Phys.* **1977**, *66* (12), 5823−5825.
(6) Crawford, O. H.; Garrett, W. R. Electron Affinities of Polar Molecules. *J. Chem. Phys.* **1977**, *66* (11), 4968−4970.
(7) Jackson, R. L.; Zimmerman, A. H.; Brauman, J. I. Resonant States at Threshold Observed in Electron Photodetachment Cross Sections of Polyatomic Negative Ions. *J. Chem. Phys.* **1979**, *71* (5), 2088−2094.
(8) Lykke, K. R.; Mead, R. D.; Lineberger, W. C. Observation of Dipole-Bound States of Negative Ions. *Phys. Rev. Lett.* **1984**, *52* (25), 2221−2224.
(9) Mead, R. D.; Lykke, K. R.; Lineberger, W. C.; Marks, J.; Brauman, J. I. Spectroscopy and Dynamics of the Dipole-bound State of Acetaldehyde Enolate. *J. Chem. Phys.* **1984**, *81* (11), 4883−4892.
(10) Gutowski, M.; Jordan, K. D.; Skurski, P. Electronic Structure of Dipole-Bound Anions. *J. Phys. Chem. A* **1998**, *102* (15), 2624−2633.
(11) Jordan, K. D.; Wang; F. Theory of Dipole-Bound Anions. *Annu. Rev. Phys. Chem.* **2003**, *54* (1), 367−396.
(12) Simons, J. Molecular Anions. *J. Phys. Chem. A* **2008**, *112* (29), 6401−6511.
(13) Jordan, K. D.; Liebman, J. F. Binding of an Electron to a Molecular Quadrupole: (BeO)2. *Chem. Phys. Lett.* **1979**, *62* (1), 143−147.
(14) Zhu, G.-Z.; Liu, Y.; Wang, L.-S. Observation of Excited Quadrupole-Bound States in Cold Anions. *Phys. Rev. Lett.* **2017**, *119* (2), 023002.
(15) Liu, G.; Ciborowski, S. M.; Pitts, C. R.; Graham, J. D.; Buytendyk, A. M.; Lectka, T.; Bowen, K. H. Observation of the Dipole- and Quadrupole-Bound Anions of 1,4-Dicyanocyclohexane. *Phys. Chem. Chem. Phys.* **2019**, *21* (33), 18310−18315.
(16) Voora, V. K.; Cederbaum, L. S.; Jordan, K. D. Existence of a Correlation Bound S-Type Anion State of C60. *J. Phys. Chem. Lett.* **2013**, *4* (6), 849−853.
(17) Klaiman, S.; Gromov, E. V.; Cederbaum, L. S. Extreme Correlation Effects in the Elusive Bound Spectrum of C60−. *J. Phys. Chem. Lett.* **2013**, *4* (19), 3319−3324.
(18) Voora, V. K.; Jordan, K. D. Nonvalence Correlation-Bound Anion States of Spherical Fullerenes. *Nano Lett.* **2014**, *14* (8), 4602−4606.
(19) Klaiman, S.; Gromov, E. V.; Cederbaum, L. S. All for One and One for All: Accommodating an Extra Electron in C60. *Phys. Chem. Chem. Phys.* **2014**, *16* (26), 13287−13293.
(20) Weber, J. M.; Ruf, M.-W.; Hotop, H. Rydberg Electron Transfer to C60 and C70. *Z. Phys. D: At., Mol. Clusters* **1996**, *37* (4), 351−357.
(21) Dąbkowska, I.; Rak, J.; Gutowski, M.; Nilles, J. M.; Stokes, S. T.; Radisic, D.; Jr, K. H. B. Barrier-Free Proton Transfer in Anionic Complex of Thymine with Glycine. *Phys. Chem. Chem. Phys.* **2004**, *6* (17), 4351−4357.
(22) Sommerfeld, T. Dipole-Bound States as Doorways in (Dissociative) Electron Attachment. *J. Phys.: Conf. Ser.* **2005**, *4* (1), 245.
(23) Voora, V. K.; Jordan, K. D. Nonvalence Correlation-Bound Anion State of C6F6: Doorway to Low-Energy Electron Capture. *J. Phys. Chem. A* **2014**, *118* (35), 7201−7205.
(24) Rogers, J. P.; Anstöter, C. S.; Verlet, J. R. R. Ultrafast Dynamics of Low-Energy Electron Attachment via a Non-Valence Correlation-Bound State. *Nat. Chem.* **2018**, *10* (3), 341−346.
(25) Sarre, P. J. The Diffuse Interstellar Bands: A Dipole-Bound State Hypothesis. *Mon. Not. R. Astron. Soc.* **2000**, *313* (1), L14−L16.
(26) Fortenberry, R. C.; Crawford, T. D. Theoretical Prediction of New Dipole-Bound Singlet States for Anions of Interstellar Interest. *J. Chem. Phys.* **2011**, *134* (15), 154304.
(27) Fortenberry, R. C. Interstellar Anions: The Role of Quantum Chemistry. *J. Phys. Chem. A* **2015**, *119* (39), 9941−9953.
(28) Turner, D. W. Molecular Photoelectron Spectroscopy. *Annu. Rev. Phys. Chem.* **1970**, *268* (1184), 7−31.

https://dx.doi.org/10.1021/acs.jpca.0c01260
J. Phys. Chem. A 2020, 124, 3507−3519

(29) Wenthold, P. G.; Lineberger, W. C. Negative Ion Photoelectron Spectroscopy Studies of Organic Reactive Intermediates. *Acc. Chem. Res.* **1999**, *32* (7), 597−604.
(30) Cyr, D. R.; Hayden, C. C. Femtosecond Time-resolved Photoionization and Photoelectron Spectroscopy Studies of Ultrafast Internal Conversion in 1,3,5-hexatriene. *J. Chem. Phys.* **1996**, *104* (2), 771−774.
(31) Stolow, A.; Bragg, A. E.; Neumark, D. M. Femtosecond Time-Resolved Photoelectron Spectroscopy. *Chem. Rev.* **2004**, *104* (4), 1719−1758.
(32) Verlet, J. R. R. Femtosecond Spectroscopy of Cluster Anions: Insights into Condensed-Phase Phenomena from the Gas-Phase. *Chem. Soc. Rev.* **2008**, *37* (3), 505−517.
(33) Blanchet, V.; Zgierski, M. Z.; Seideman, T.; Stolow, A. Discerning Vibronic Molecular Dynamics Using Time-Resolved Photoelectron Spectroscopy. *Nature* **1999**, *401* (6748), 52−54.
(34) Eppink, A. T. J. B.; Parker, D. H. Velocity Map Imaging of Ions and Electrons Using Electrostatic Lenses: Application in Photoelectron and Photofragment Ion Imaging of Molecular Oxygen. *Rev. Sci. Instrum.* **1997**, *68* (9), 3477−3484.
(35) Reid, K. L. Photoelectron Angular Distributions. *Annu. Rev. Phys. Chem.* **2003**, *54* (1), 397−424.
(36) Mabbs, R.; Grumbling, E. R.; Pichugin, K.; Sanov, A. Photoelectron Imaging: An Experimental Window into Electronic Structure. *Chem. Soc. Rev.* **2009**, *38* (8), 2169−2177.
(37) Sanov, A. Laboratory-Frame Photoelectron Angular Distributions in Anion Photodetachment: Insight into Electronic Structure and Intermolecular Interactions. *Annu. Rev. Phys. Chem.* **2014**, *65* (1), 341−363.
(38) Anstöter, C. S.; Dean, C. R.; Verlet, J. R. R. Chromophores of Chromophores: A Bottom-up Hückel Picture of the Excited States of Photoactive Proteins. *Phys. Chem. Chem. Phys.* **2017**, *19* (44), 29772−29779.
(39) Stanley, L. H.; Anstöter, C. S.; Verlet, J. R. R. Resonances of the Anthracenyl Anion Probed by Frequency-Resolved Photoelectron Imaging of Collision-Induced Dissociated Anthracene Carboxylic Acid. *Chem. Sci.* **2017**, *8* (4), 3054−3061.
(40) Anstöter, C. S.; Dean, C. R.; Verlet, J. R. R. Sensitivity of Photoelectron Angular Distributions to Molecular Conformations of Anions. *J. Phys. Chem. Lett.* **2017**, *8* (10), 2268−2273.
(41) Cooper, J.; Zare, R. N. Angular Distribution of Photoelectrons. *J. Chem. Phys.* **1968**, *48* (2), 942−943.
(42) Bailey, C. G.; Dessent, C. E. H.; Johnson, M. A.; Bowen, K. H. Vibronic Effects in the Photon Energy-dependent Photoelectron Spectra of the CH3CN− Dipole-bound Anion. *J. Chem. Phys.* **1996**, *104* (18), 6976−6983.
(43) Hendricks, J. H.; Lyapustina, S. A.; de Clercq, H. L.; Snodgrass, J. T.; Bowen, K. H. Dipole Bound, Nucleic Acid Base Anions Studied via Negative Ion Photoelectron Spectroscopy. *J. Chem. Phys.* **1996**, *104* (19), 7788−7791.
(44) Diken, E. G.; Hammer, N. I.; Johnson, M. A. Preparation and Photoelectron Spectrum of the Glycine Molecular Anion: Assignment to a Dipole-Bound Electron Species with a High-Dipole Moment, Non-Zwitterionic Form of the Neutral Core. *J. Chem. Phys.* **2004**, *120* (21), 9899−9902.
(45) Adams, C. L.; Knurr, B. J.; Weber, J. M. Photoelectron Spectroscopy of 1-Nitropropane and 1-Nitrobutane Anions. *J. Chem. Phys.* **2012**, *136* (6), 064307.
(46) Belogolova, E. F.; Liu, G.; Doronina, E. P.; Ciborowski, S. M.; Sidorkin, V. F.; Bowen, K. H. Dipole-Bound Anions of Intramolecular Complexes. *J. Phys. Chem. Lett.* **2018**, *9* (6), 1284−1289.
(47) Ciborowski, S. M.; Liu, G.; Graham, J. D.; Buytendyk, A. M.; Bowen, K. H. Dipole-Bound Anions: Formed by Rydberg Electron Transfer (RET) and Studied by Velocity Map Imaging−Anion Photoelectron Spectroscopy (VMI−APES). *Eur. Phys. J. D* **2018**, *72* (8), 139.
(48) Lecointre, J.; Roberts, G. M.; Horke, D. A.; Verlet, J. R. R. Ultrafast Relaxation Dynamics Observed Through Time-Resolved Photoelectron Angular Distributions. *J. Phys. Chem. A* **2010**, *114* (42), 11216−11224.
(49) Rogers, J. P.; Anstöter, C. S.; Bull, J. N.; Curchod, B. F. E.; Verlet, J. R. R. Photoelectron Spectroscopy of the Hexafluorobenzene Cluster Anions: (C6F6)n− (n = 1−5) and I−(C6F6). *J. Phys. Chem. A* **2019**, *123* (8), 1602−1612.
(50) Horke, D. A.; Roberts, G. M.; Lecointre, J.; Verlet, J. R. R. Velocity-Map Imaging at Low Extraction Fields. *Rev. Sci. Instrum.* **2012**, *83* (6), 063101.
(51) Allan, M.; Regeta, K.; Gorfinkiel, J. D.; Mašín, Z.; Grimme, S.; Bannwarth, C. Recent Research Directions in Fribourg: Nuclear Dynamics in Resonances Revealed by 2-Dimensional EEL Spectra, Electron Collisions with Ionic Liquids and Electronic Excitation of Pyrimidine. *Eur. Phys. J. D* **2016**, *70* (5), 123.
(52) West, C. W.; Bull, J. N.; Antonkov, E.; Verlet, J. R. R. Anion Resonances of Para-Benzoquinone Probed by Frequency-Resolved Photoelectron Imaging. *J. Phys. Chem. A* **2014**, *118* (48), 11346−11354.
(53) Bull, J. N.; West, C. W.; Verlet, J. R. R. On the Formation of Anions: Frequency-, Angle-, and Time-Resolved Photoelectron Imaging of the Menadione Radical Anion. *Chem. Sci.* **2015**, *6* (2), 1578−1589.
(54) Bull, J. N.; West, C. W.; Verlet, J. R. R. Anion Resonances and Above-Threshold Dynamics of Coenzyme Q0. *Phys. Chem. Chem. Phys.* **2015**, *17* (24), 16125−16135.
(55) Anstöter, C. S.; Gartmann, T. E.; Stanley, L. H.; Bochenkova, A. V.; Verlet, J. R. R. Electronic Structure of the Para-Dinitrobenzene Radical Anion: A Combined 2D Photoelectron Imaging and Computational Study. *Phys. Chem. Chem. Phys.* **2018**, *20* (37), 24019−24026.
(56) West, C. W.; Bull, J. N.; Hudson, A. S.; Cobb, S. L.; Verlet, J. R. R. Excited State Dynamics of the Isolated Green Fluorescent Protein Chromophore Anion Following UV Excitation. *J. Phys. Chem. B* **2015**, *119* (10), 3982−3987.
(57) Bull, J. N.; West, C. W.; Verlet, J. R. R. Ultrafast Dynamics of Formation and Autodetachment of a Dipole-Bound State in an Open-Shell π-Stacked Dimer Anion. *Chem. Sci.* **2016**, *7* (8), 5352−5361.
(58) Bull, J. N.; Verlet, J. R. R. Dynamics of Π*-Resonances in Anionic Clusters of Para-Toluquinone. *Phys. Chem. Chem. Phys.* **2017**, *19* (39), 26589−26595.
(59) Bull, J. N.; Verlet, J. R. R. Observation and Ultrafast Dynamics of a Nonvalence Correlation-Bound State of an Anion. *Sci. Adv.* **2017**, *3* (5), No. e1603106.
(60) Mensa-Bonsu, G.; Lietard, A.; Verlet, J. R. R. Enhancement of Electron Accepting Ability of Para-Benzoquinone by a Single Water Molecule. *Phys. Chem. Chem. Phys.* **2019**, *21* (39), 21689−21692.
(61) Mensa-Bonsu, G.; Tozer, D. J.; Verlet, J. R. R. Photoelectron Spectroscopic Study of I−·ICF3: A Frontside Attack SN2 Pre-Reaction Complex. *Phys. Chem. Chem. Phys.* **2019**, *21* (26), 13977−13985.
(62) Rogers, J. P.; Anstöter, C. S.; Verlet, J. R. R. Evidence of Electron Capture of an Outgoing Photoelectron Wave by a Nonvalence State in (C6F6)n−. *J. Phys. Chem. Lett.* **2018**, *9* (10), 2504−2509.
(63) Anstöter, C. S.; Bull, J. N.; Verlet, J. R. R. Ultrafast Dynamics of Temporary Anions Probed through the Prism of Photodetachment. *Int. Rev. Phys. Chem.* **2016**, *35* (4), 509−538.
(64) Horke, D. A.; Li, Q.; Blancafort, L.; Verlet, J. R. R. Ultrafast Above-Threshold Dynamics of the Radical Anion of a Prototypical Quinone Electron-Acceptor. *Nat. Chem.* **2013**, *5* (8), 711−717.
(65) Campbell, E. E. B.; Levine, R. D. Delayed Ionization and Fragmentation En Route to Thermionic Emission: Statistics and Dynamics. *Annu. Rev. Phys. Chem.* **2000**, *51* (1), 65−98.
(66) Andersen, J. U.; Bonderup, E.; Hansen, K. Thermionic Emission from Clusters. *J. Phys. B At. Mol. Opt. Phys.* **2002**, *35* (5), R1.
(67) Adams, C. L.; Hansen, K.; Weber, J. M. Vibrational Autodetachment from Anionic Nitroalkane Chains: From Molecular

https://dx.doi.org/10.1021/acs.jpca.0c01260
J. Phys. Chem. A 2020, 124, 3507−3519

Signatures to Thermionic Emission. *J. Phys. Chem. A* **2019**, *123* (40), 8562−8570.
(68) Simons, J. Propensity Rules for Vibration-Induced Electron Detachment of Anions. *J. Am. Chem. Soc.* **1981**, *103* (14), 3971−3976.
(69) Zhu, G.-Z.; Wang, L.-S. High-Resolution Photoelectron Imaging and Resonant Photoelectron Spectroscopy via Noncovalently Bound Excited States of Cryogenically Cooled Anions. *Chem. Sci.* **2019**, *10* (41), 9409−9423.
(70) Horke, D. A.; Verlet, J. R. R. Photoelectron Spectroscopy of the Model GFP Chromophore Anion. *Phys. Chem. Chem. Phys.* **2012**, *14* (24), 8511−8515.
(71) Zagorec-Marks, W.; Foreman, M. M.; Verlet, J. R. R.; Weber, J. M. Cryogenic Ion Spectroscopy of the Green Fluorescent Protein Chromophore in Vacuo. *J. Phys. Chem. Lett.* **2019**, *10* (24), 7817−7822.
(72) Mooney, C. R. S.; Horke, D. A.; Chatterley, A. S.; Simperler, A.; Fielding, H. H.; Verlet, J. R. R. Taking the Green Fluorescence out of the Protein: Dynamics of the Isolated GFP Chromophore Anion. *Chem. Sci.* **2013**, *4* (3), 921−927.
(73) Lee, I.-R.; Lee, W.; Zewail, A. H. Primary Steps of the Photoactive Yellow Protein: Isolated Chromophore Dynamics and Protein Directed Function. *Proc. Natl. Acad. Sci. U. S. A.* **2006**, *103* (2), 258−262.
(74) Bull, J. N.; Anstöter, C. S.; Verlet, J. R. R. Ultrafast Valence to Non-Valence Excited State Dynamics in a Common Anionic Chromophore. *Nat. Commun.* **2019**, *10* (1), 1−9.
(75) Curchod, B. F. E.; Martínez, T. J. Ab Initio Nonadiabatic Quantum Molecular Dynamics. *Chem. Rev.* **2018**, *118* (7), 3305−3336.
(76) Wigner, E. P. On the Behavior of Cross Sections Near Thresholds. *Phys. Rev.* **1948**, *73* (9), 1002−1009.
(77) Cyr, D. M.; Bishea, G. A.; Scarton, M. G.; Johnson, M. A. Observation of Charge-transfer Excited States in the I−·CH3I, I−·CH3Br, and I−·CH2Br2SN2 Reaction Intermediates Using Photofragmentation and Photoelectron Spectroscopies. *J. Chem. Phys.* **1992**, *97* (8), 5911−5914.
(78) Cyr, D. M.; Scarton, M. G.; Johnson, M. A. Photoelectron Spectroscopy of the Gas-phase SN2 Reaction Intermediates I−·CH3I and I−·CD3I: Distortion of the CH3I at the "'Ion−Dipole"' Complex. *J. Chem. Phys.* **1993**, *99* (6), 4869−4872.
(79) Dessent, C. E. H.; Bailey, C. G.; Johnson, M. A. Photoinitiation of the Anionic Condensation Reaction in 2-Chloroacrylonitrile via the Charge-Transfer Bands of the Cl−·(2-Chloroacrylonitrile)1,2 Clusters. *Chem. Phys. Lett.* **1995**, *244* (1), 127−132.
(80) Dessent, C. E. H.; Bailey, C. G.; Johnson, M. A. Dipole-bound Excited States of the I−·CH3CN and I−·(CH3CN)2 Ion−Molecule Complexes: Evidence for Asymmetric Solvation. *J. Chem. Phys.* **1995**, *103* (6), 2006−2015.
(81) Dessent, C. E. H.; Bailey, C. G.; Johnson, M. A. Observation of the Dipole-bound Excited State of the I−·acetone Ion−molecule Complex. *J. Chem. Phys.* **1995**, *102* (15), 6335−6338.
(82) Serxner, D.; Dessent, C. E. H.; Johnson, M. A. Precursor of the Iaq− Charge-transfer-to-solvent (CTTS) Band in I−·(H2O)n Clusters. *J. Chem. Phys.* **1996**, *105* (16), 7231−7234.
(83) Dessent, C. E. H.; Johnson, M. A. Photoinitiation of Gas-Phase SN2 Reactions through the Evans−Polanyi Excited State Surface. *J. Am. Chem. Soc.* **1997**, *119* (21), 5067−5068.
(84) Bradforth, S. E.; Jungwirth, P. Excited States of Iodide Anions in Water: A Comparison of the Electronic Structure in Clusters and in Bulk Solution. *J. Phys. Chem. A* **2002**, *106* (7), 1286−1298.
(85) Lehr, L.; Zanni, M. T.; Frischkorn, C.; Weinkauf, R.; Neumark, D. M. Electron Solvation in Finite Systems: Femtosecond Dynamics of Iodide·(Water)n Anion Clusters. *Science* **1999**, *284* (5414), 635−638.
(86) Verlet, J. R. R.; Kammrath, A.; Griffin, G. B.; Neumark, D. M. Electron Solvation in Water Clusters Following Charge Transfer from Iodide. *J. Chem. Phys.* **2005**, *123* (23), 231102.
(87) Kammrath, A.; Verlet, J. R. R.; Bragg, A. E.; Griffin, G. B.; Neumark, D. M. Dynamics of Charge-Transfer-to-Solvent Precursor States in I-(Water)n (n = 3−10) Clusters Studied with Photoelectron Imaging. *J. Phys. Chem. A* **2005**, *109* (50), 11475−11483.
(88) Yandell, M. A.; King, S. B.; Neumark, D. M. Decay Dynamics of Nascent Acetonitrile and Nitromethane Dipole-Bound Anions Produced by Intracluster Charge-Transfer. *J. Chem. Phys.* **2014**, *140* (18), 184317.
(89) Yandell, M. A.; King, S. B.; Neumark, D. M. Time-Resolved Radiation Chemistry: Photoelectron Imaging of Transient Negative Ions of Nucleobases. *J. Am. Chem. Soc.* **2013**, *135* (6), 2128−2131.
(90) Stephansen, A. B.; King, S. B.; Yokoi, Y.; Minoshima, Y.; Li, W.-L.; Kunin, A.; Takayanagi, T.; Neumark, D. M. Dynamics of Dipole- and Valence Bound Anions in Iodide-Adenine Binary Complexes: A Time-Resolved Photoelectron Imaging and Quantum Mechanical Investigation. *J. Chem. Phys.* **2015**, *143* (10), 104308.
(91) Li, W.-L.; Kunin, A.; Matthews, E.; Yoshikawa, N.; Dessent, C. E. H.; Neumark, D. M. Photodissociation Dynamics of the Iodide-Uracil (I−U) Complex. *J. Chem. Phys.* **2016**, *145* (4), 044319.
(92) Kunin, A.; Neumark, D. M. Time-Resolved Radiation Chemistry: Femtosecond Photoelectron Spectroscopy of Electron Attachment and Photodissociation Dynamics in Iodide−Nucleobase Clusters. *Phys. Chem. Chem. Phys.* **2019**, *21* (14), 7239−7255.
(93) Nakajima, A.; Taguwa, T.; Hoshino, K.; Sugioka, T.; Naganuma, T.; Oho, F.; Watanabe, K.; Nakao, K.; Konishi, Y.; Kishi, R.; Kaya, K. Photoelectron Spectroscopy of (C6F6)−n and (Au-C6F6)− Clusters. *Chem. Phys. Lett.* **1993**, *214* (1), 22−26.
(94) Verlet, J. R. R.; Kammrath, A.; Griffin, G. B.; Neumark, D. M. Electron Solvation in Water Clusters Following Charge Transfer from Iodide. *J. Chem. Phys.* **2005**, *123* (23), 231102.
(95) Verlet, J. R. R.; Bragg, A. E.; Kammrath, A.; Cheshnovsky, O.; Neumark, D. M. Observation of Large Water-Cluster Anions with Surface-Bound Excess Electrons. *Science* **2005**, *307* (5706), 93−96.
(96) Lietard, A.; Verlet, J. R. R. Selectivity in Electron Attachment to Water Clusters. *J. Phys. Chem. Lett.* **2019**, *10* (6), 1180−1184.
(97) Messina, F.; Bräm, O.; Cannizzo, A.; Chergui, M. Real-Time Observation of the Charge Transfer to Solvent Dynamics. *Nat. Commun.* **2013**, *4* (1), 1−6.
(98) Sagar, D. M.; Bain, Colin. D.; Verlet, J. R. R. Hydrated Electrons at the Water/Air Interface. *J. Am. Chem. Soc.* **2010**, *132* (20), 6917−6919.
(99) Nowakowski, P. J.; Woods, D. A.; Verlet, J. R. R. Charge Transfer to Solvent Dynamics at the Ambient Water/Air Interface. *J. Phys. Chem. Lett.* **2016**, *7* (20), 4079−4085.
(100) Zhu, G.-Z.; Cheung, L. F.; Liu, Y.; Qian, C.-H.; Wang, L.-S. Resonant Two-Photon Photoelectron Imaging and Intersystem Crossing from Excited Dipole-Bound States of Cold Anions. *J. Phys. Chem. Lett.* **2019**, *10* (15), 4339−4344.
(101) Jagau, T.-C.; Bravaya, K. B.; Krylov, A. I. Extending Quantum Chemistry of Bound States to Electronic Resonances. *Annu. Rev. Phys. Chem.* **2017**, *68* (1), 525−553.
(102) Chen, X.; Bradforth, S. E. The Ultrafast Dynamics of Photodetachment. *Annu. Rev. Phys. Chem.* **2008**, *59* (1), 203−231.
(103) Henley, A.; Fielding, H. H. Anion Photoelectron Spectroscopy of Protein Chromophores. *Int. Rev. Phys. Chem.* **2019**, *38* (1), 1−34.
(104) Nielsen, S. B.; Lapierre, A.; Andersen, J. U.; Pedersen, U. V.; Tomita, S.; Andersen, L. H. Absorption Spectrum of the Green Fluorescent Protein Chromophore Anion In Vacuo. *Phys. Rev. Lett.* **2001**, *87* (22), 228102.
(105) Ormö, M.; Cubitt, A. B.; Kallio, K.; Gross, L. A.; Tsien, R. Y.; Remington, S. J. Crystal Structure of the Aequorea Victoria Green Fluorescent Protein. *Science* **1996**, *273* (5280), 1392−1395.
(106) Castellani, M. E.; Anstöter, C. S.; Verlet, J. R. R. On the Stability of a Dipole-Bound State in the Presence of a Molecule. *Phys. Chem. Chem. Phys.* **2019**, *21* (44), 24286−24290.
(107) Sommerfeld, T.; Davis, M. C. Excluded-Volume Descriptors for Dipole-Bound Anions: Amine N-Oxides as a Test Case. *J. Chem. Phys.* **2020**, *152* (5), 054102.

https://dx.doi.org/10.1021/acs.jpca.0c01260
J. Phys. Chem. A 2020, 124, 3507−3519

(108) Bogdanov, A. M.; Mishin, A. S.; Yampolsky, I. V.; Belousov, V. V.; Chudakov, D. M.; Subach, F. V.; Verkhusha, V. V.; Lukyanov, S.; Lukyanov, K. A. Green Fluorescent Proteins Are Light-Induced Electron Donors. *Nat. Chem. Biol.* **2009**, *5* (7), 459−461.
(109) Bochenkova, A. V.; Andersen, L. H. Ultrafast Dual Photoresponse of Isolated Biological Chromophores: Link to the Photoinduced Mode-Specific Non-Adiabatic Dynamics in Proteins. *Faraday Discuss.* **2013**, *163* (0), 297−319.
(110) Bochenkova, A. V.; Mooney, C. R. S.; Parkes, M. A.; Woodhouse, J. L.; Zhang, L.; Lewin, R.; Ward, J. M.; Hailes, H. C.; Andersen, L. H.; Fielding, H. H. Mechanism of Resonant Electron Emission from the Deprotonated GFP Chromophore and Its Biomimetics. *Chem. Sci.* **2017**, *8* (4), 3154−3163.

https://dx.doi.org/10.1021/acs.jpca.0c01260
J. Phys. Chem. A 2020, 124, 3507−3519